CDDpress

www.nature.com/cddis

ARTICLE OPEN

Downregulation of the Rho GTPase pathway abrogates resistance to ionizing radiation in wild-type p53 glioblastoma by suppressing DNA repair mechanisms

Yuli Thamires Magalhaes[1,2], Viktor Kalbermatter Boell[1], Giovanna Duo Cardella[1] and Fabio Luis Forti[1]✉

Glioblastoma (GBM), the most common aggressive brain tumor, is characterized by rapid cellular infiltration and is routinely treated with ionizing radiation (IR), but therapeutic resistance inevitably recurs. The actin cytoskeleton of glioblastoma cells provides their high invasiveness, but it remains unclear whether Rho GTPases modulate DNA damage repair and therapeutic sensitivity. Here, we irradiated glioblastoma cells with different p53 status and explored the effects of Rho pathway inhibition to elucidate how actin cytoskeleton disruption affects the DNA damage response and repair pathways. p53-wild-type and p53-mutant cells were subjected to Rho GTPase pathway modulation by treatment with C3 toxin; knockdown of mDia-1, PFN1 and MYPT1; or treatment with F-actin polymerization inhibitors. Rho inhibition increased the sensitivity of glioma cells to IR by increasing the number of DNA double-strand breaks and delaying DNA repair by nonhomologous end-joining in p53-wild-type cells. p53 knockdown reversed this phenotype by reducing p21 expression and Rho signaling activity, whereas reactivation of p53 in p53-mutant cells by treatment with PRIMA-1 reversed these effects. The interdependence between p53 and Rho is based on nuclear p53 translocation facilitated by G-actin and enhanced by IR. Isolated IR-resistant p53-wild-type cells showed an altered morphology and increased stress fiber formation: inhibition of Rho or actin polymerization decreased cell viability in a p53-dependent manner and reversed the resistance phenotype. p53 silencing reversed the Rho inhibition-induced sensitization of IR-resistant cells. Rho inhibition also impaired the repair of IR-damaged DNA in 3D spheroid models. Rho GTPase activity and actin cytoskeleton dynamics are sensitive targets for the reversal of acquired resistance in GBM tumors with wild-type p53.

Cell Death and Disease (2023)14:283 ; https://doi.org/10.1038/s41419-023-05812-1

INTRODUCTION

Among primary brain tumors, glioblastoma (GBM, WHO grade IV astrocytoma) remains the most common (accounting for 14.5% of all brain tumors and 57.7% of gliomas) and most malignant, with a dismal prognosis characterized by an average survival time of 15 months and a patient survival rate of <10% in the five years after diagnosis [1, 2]. GBM is among the solid tumors with the greatest resistance to radiotherapy, which directly contributes to its poor prognosis, since the majority of patients experience tumor recurrence within 2 years [3, 4]. Several mechanisms are involved in GBM radioresistance, including DNA damage and repair [5, 6], which is involved mainly by activating DNA damage response (DDR) signaling and inducing double strand break (DSB) repair by both homologous recombination (HR) and nonhomologous end joining (NHEJ) [7].

Another well-described factor for the acquisition of radioresistance in GBM is the tumor suppressor p53, which is central to the network controlling cell proliferation, survival, and genome integrity. p53 is one of the most frequently mutated genes in human cancers (40% to 50% of GBMs have p53 mutations), and unlike most tumor suppressors, p53 is rarely deleted in GBM, since its alterations are mostly missense mutations in the DNA binding domain, leading to inhibition of its transcription factor activity [7, 8]. In fact, mutant p53 proteins are highly expressed in GBM, and the lack of p53-mediated apoptosis is crucial for GBM resistance, since the failure of p53 to induce p21 expression promotes radioresistance in GBM cells [7]. Thus, interest in elucidating the mechanism that drives GBM radioresistance has increased, with special focus on the different processes that modulate DNA damage signaling and repair in the search for novel targets for GBM radiosensitization [9].

The Rho GTPase pathway is well known for regulating cell proliferation and differentiation, actin cytoskeleton dynamics and cell motility. This pathway is commonly deregulated in GBM, since an increase in the activity of RhoA, as well as the other members of the Rho GTPase family, or overexpression of guanine exchange factors (GEFs) promotes the migration and invasion of these cells. The high invasiveness of GBM is one of the major obstacles to clinical therapy, as these cells are intrinsically more resistant to current therapies [10]. All typical Rho GTPases have been shown to act in the early stages of DNA damage recognition, mainly through regulation of DDR pathways [11–15], and are also activated in response to genotoxic stressors [16, 17]. Therefore, higher Rho GTPase activity seems to be necessary for DDR

[1]Laboratory of Biomolecular Systems Signaling, Department of Biochemistry, Institute of Chemistry, University of São Paulo, São Paulo, Brazil. [2]These authors contributed equally: Yuli Thamires Magalhaes. ✉email: flforti@iq.usp.br

Received: 5 October 2022 Revised: 9 March 2023 Accepted: 13 April 2023
Published online: 21 April 2023

signaling and efficient repair of DSBs, among other types of DNA lesions [11, 13, 15–18]. The relationship between Rho and the p53 pathway has been pointed out in recent years and is purported to exert effects mainly via regulation of the cell cycle [19–22], gene expression [23–25] and cell migration [26, 27]; however, the mechanism and interdependence of these pathways in DNA repair and tumor resistance have not yet been sufficiently explored and demonstrated.

In this study, we investigated the contributions of the Rho pathway and actin cytoskeleton dynamics in the acquisition of ionizing radiation (IR) resistance in GBM and their potential interdependence with the p53 status in terms of its association with DNA damage response and repair pathways. We generated IR-resistant cells through continuous cycles of IR exposure and analyzed changes in the Rho and DDR pathways during radioresistance acquisition. Our findings demonstrate the mechanism by which inhibition of Rho GTPases and actin polymerization promote efficient sensitization of GBM cells expressing wild-type p53 to treatment with IR, and they suggest these pathways as targets for the reversal of acquired radioresistance in GBM tumors, with the advantage of simultaneously addressing the high invasiveness of GBM cells.

MATERIALS AND METHODS

Bioinformatics analysis

The gene expression in the patient tumor sample set and survival analysis data obtained by the Kaplan–Meier method were obtained from the GEPIA2 platform (http://gepia2.cancer-pku.cn) using the TCGA database for GBM and LGG data and the GTEx database for normal tissue data. The gene expression profiles of GBM cells were obtained from the Cancer Cell Line Encyclopedia (CCLE) transcriptome database via the EMBL Cell Expression Atlas platform (https://www.ebi.ac.uk/gxa/home).

GBM cell lines and culture conditions

The GBM cell lines U87-MG, A172 and U343-MG (p53- wild-type) and T98G, U138-MG and U251-MG (p53- mutated) were obtained from American Type Culture Collection (ATCC) and kindly provided by Prof. Dr. Carlos Frederico Martins Menck (ICB-USP), Prof. Dr. Mari Cleide Sogayar (IQUSP e FMUSP) and Prof. Dr. Elza Tiemi Sakamoto Hojo (FFCLRP-USP). All cells were cultured in DMEM supplemented with 10% FBS, 25 µg/mL ampicillin and 100 µg/mL streptomycin at 37 °C and 5% CO_2 for up to a maximum of 4 weeks and were monitored by frequent genotypic and phenotypic characterization in addition to testing for mycoplasma contamination, thus ensuring the quality of the model.

Drugs and treatments

Cells were subjected to Rho inhibition by transient transfection of a vector containing the C3 toxin coding sequence, as previously described [15], or gene silencing by transfection of siRNAs specific for mDia1, PFN1, MYPT1 or p53 (MISSION® esiRNA, Invitrogen) using Lipofectamine 3000 (Invitrogen) according to the manufacturer's protocol. Rho activity was also modulated by 48 h of starvation in serum-free medium prior to activation with medium containing 30% FBS. F-actin disruption was performed by treatment with cytochalasin D (Sigma–Aldrich) diluted directly in the medium at the desired concentration and for the desired time of exposure. The activity of mutant p53 was restored by treatment with the agent PRIMA-1 (Sigma–Aldrich), diluted directly in the medium to the indicated concentration, for 24 h. The efficiency of p53 reactivation was determined by measuring p21 expression and transfection of a luciferase reporter gene fused to a p53-responsive promoter [28]. To simulate radiotherapy, GBM cells were exposed to gamma ionizing radiation as previously described [16] at the Nuclear and Energy Research Institute (IPEN, SP, Brazil).

Rho activity assay and immunoblotting

Rho activity was measured by a pulldown assay, as previously described [16]. Briefly, cellular protein extracts (DTT-free) were incubated with glutathione-Sepharose beads bound to the RBD-GST fusion protein. After the wash steps and recovery by centrifugation, the proportion of Rho-GTP bound to RBD-GST was quantified by immunoblotting as described [15] here in brief: specific amounts of protein extracts (quantified by the Bradford method) were denatured with the Laemmli protocol, separated by SDS–PAGE and transferred to a nitrocellulose membrane (Millipore). After blocking with 5% low-fat milk/TBS-T for 30 min, the membranes were incubated with specific primary and secondary antibodies under the optimized incubation conditions described in the Supplementary data. Band density quantification was performed in ImageJ.

Survival analysis by a soft agar colony formation assay

For the clonogenic assays [15], pretreated cells were mixed with 0.3% agarose/medium at a low cellular density and rapidly plated in 48-well plates precoated with a thin layer of 0.6% agarose/medium. Complete medium was added on top of the layer after agarose solidification and replaced every 2 days until the emergence of visible colonies, which were then photographed and counted.

Alkaline comet assay

The comet assay for the detection of DNA fragmentation was performed as previously described [16, 29]. In summary, cells were collected at several time points after IR exposure, mixed with 0.5% low-melting point agarose and scattered onto glass slides covered with a thin layer of normal agarose. Then, the cells were lysed and deproteinated, and the DNA was denatured and subjected to single-cell electrophoresis. Slides were then placed in neutralization buffer (Tris, pH 7.4) and fixed with pure ethanol. DNA was stained with SYBR Green II (Invitrogen), and the comet assay data were analyzed using Comet Assay IV software (Instem).

Analysis of γH2AX(Ser139), 53BP1, phospho-ATM (Ser1981) and phospho-NBS1 (Ser343) foci

Immunofluorescence assays were performed as described before with adaptations [13]. In brief, cells were seeded on round glass coverslips and treated as desired. Then, the cells were fixed with 4% PFA for 10 min and permeabilized with 0,5% Triton X-100 for 5 min on ice. The samples were blocked with 10% FBS/3% albumin in PBS for 30 min prior to antibody incubation, as described in the Supplementary data. Image acquisition was performed with a Zeiss Axio Observer 7 microscope using a 40x objective, and quantification of foci was performed with the Tissue Gnostics system [30].

NHEJ repair assay

The rate of NHEJ repair was quantified using U87-MG and T98G cells expressing the EJ5-GFP reporter, as described previously [29]. Briefly, cells stably expressing the reporter gene were obtained by transfection with Lipofectamine 3000 followed by selection and clone isolation with 5 µg/mL puromycin. For the NHEJ assay, the clones were transfected with the I-SceI expression vector or empty vector, and 72 h after transfection, the percentage of GFP-positive cells was determined by the Thermo Fisher Countess II FL automated cell counter.

p53 localization analysis

The p53 localization analysis was performed with the TissueGnostics system as previously described [30] with modifications. For this assay, cells were plated in black 96-well microplates with a transparent bottom suitable for microscopy and subjected to immunofluorescence staining as previously described. Images were acquired with a 20x objective, and DAPI images were used to generate the nuclear mask, while the p53 outline staining was used as the cytoplasmic mask for an individual cell. Using both masks, the p53 intensity in each mask was measured, and the percentages of nuclear and cytoplasmic p53 were calculated for each of 2000 cells/condition.

Generation and characterization of IR-resistant U87-MG GBM cells

To generate U87-MG IR-resistant cells, cells were divided into groups of cells in small culture bottles and subjected to different radiation exposure regimens. After each irradiation treatment, the cells were washed 3 times with PBS and returned to culture in standard medium. All cells were monitored daily regarding viability, confluence and sterility. Finally, IR-resistant cells were stored at −80 °C for at least 2 weeks before further resistance assays. To verify the resistance phenotype, cells were subjected to an MTT viability assay, where the dose–response curves were constructed and the LD50 values obtained in the presence and absence of Rho inhibition and/or p53 knockdown. Finally, immunoblotting and immunofluorescence staining for F-actin structures (Supplementary Data) were performed to complete the cell characterization.

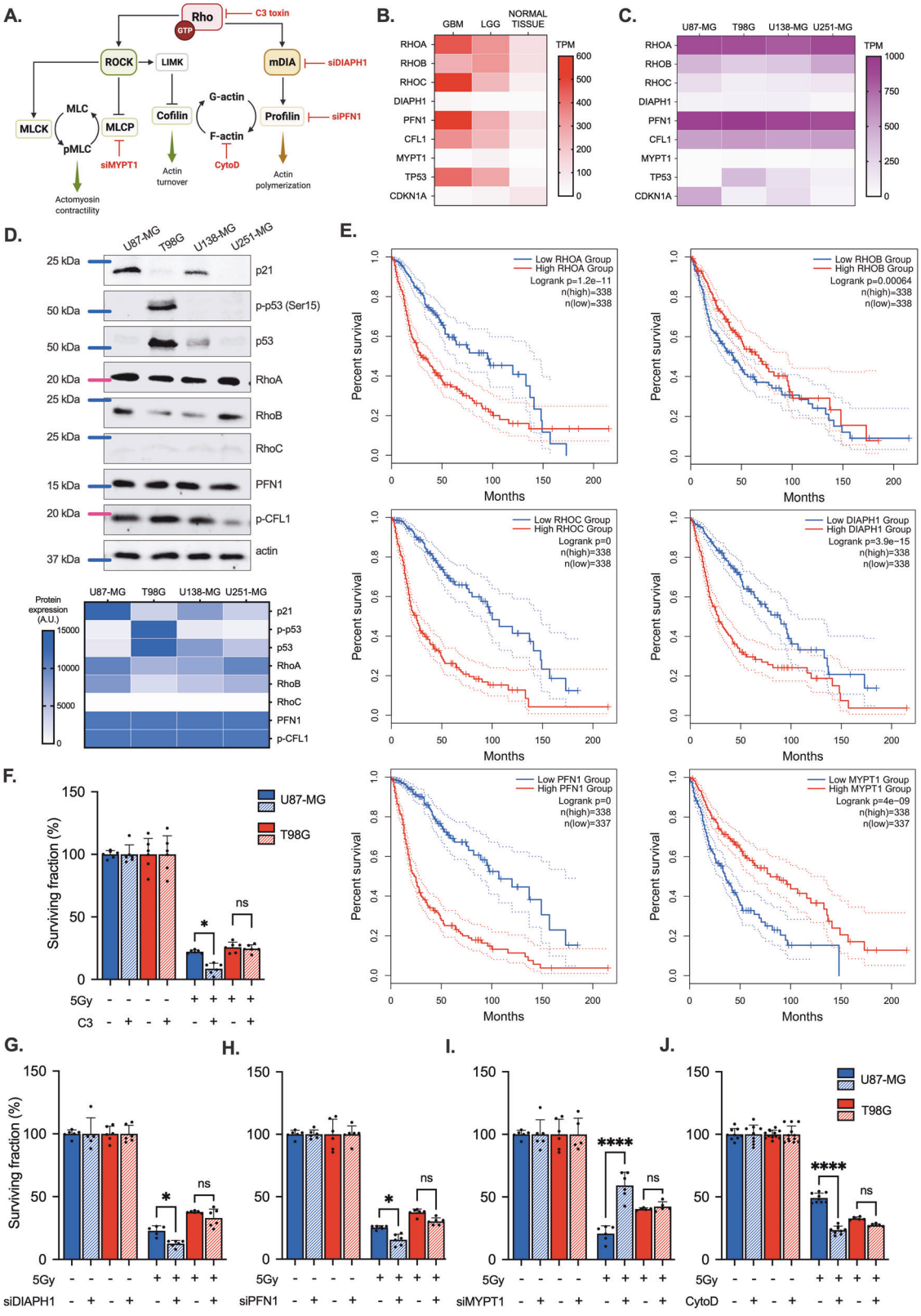

Statistical analysis

All experiments were performed with at least three independent biological replicates of two to six technical replicates each. The exact numbers of biological replicates (*N*) are noted in the figure legends, and each replicate is shown in each graph as an individual dot. Outliers were identified using the ROUT method with $Q = 1\%$. Comparisons between treatments were performed by two-way ANOVA with Tukey's or Sidak's post hoc test for multiple comparisons or by one-way ANOVA for two-group comparisons using GraphPad Prism 9 software. Differences were considered statistically significant and denoted as (*) when $0.05 \geq p > 0.001$, (**) when

Fig. 1 Targeting components of the Rho pathway reduces the viability of glioma cells. A Inhibition nodes in the Rho-mediated signaling circuit used in this work. Created with BioRender.com. **B** Differential expression of Rho pathway genes in GBM and LGG (low-grade glioma) tumor tissues compared to normal tissue: RHOA, RHOC, DIAPH1, and PFN1 are more highly expressed in high-grade gliomas, while RHOB and MYPT1 expression is lower in these tumors. Data were acquired with the GEPIA2 platform from the GTEx and TCGA databases. **C** mRNA expression data obtained from the EMBL-EBI Expression Atlas using the Cancer Cell Line Encyclopedia (CCLE) for Rho pathway components show similar expression profiles in GBM cell lines with wild-type p53 (U87-MG) and mutant p53 (T98G, U138-MG, U251-MG), while their protein expression levels are substantially different (**D**). The immunoblots are representative of at least three independent experiments. The replicate blots are available in the Original Data File. **E** Survival analysis indicates high expression of RHOA, RHOC, DIAPH1, and PFN1 and low expression of RHOB and MYPT1 as markers of poor prognosis in GBM patients. Data were obtained from the TCGA database using the GEPIA2 platform. Clonogenic survival assay of U87-MG and T98G cells with Rho pathway modulation induced by C3 toxin treatment (**F**) or knockdown of DIAPH1 (**G**), PFN1 (**H**), or MYPT1 (**I**) and subsequent treatment with IR. Inhibition of the Rho pathway decreases the survival of only wild-type p53 cells, whereas Rho pathway activation by MYPT1 knockdown increases cell survival in response to IR. **J** Treatment with the F-actin polymerization inhibitor cytochalasin D (CytoD) decreases cell survival in response to IR in U87-MG cells but not in T98G cells. The graphs show the mean ± SD of six independent experiments, with the averages of individual biological replicate dots from two colony wells, as analyzed by two-way ANOVA with Tukey's multiple comparison test.

$0.01 \geq p > 0.001$, (***) when $0.001 \geq p \geq 0.0001$, and (****) when $p < 0.0001$. Statistical analysis was performed between control and RhoA LoF cells under the same treatment conditions.

RESULTS

Targeting the Rho pathway and actin polymerization potentiates the effects of ionizing radiation on gliomas

A premise of our work is that upregulation of the Rho pathway is associated with high-grade glioma and poor prognosis. Therefore, to target key components of the Rho circuitry by using different strategies (in red, Fig. 1A), we purposely mined databases of gene expression (GTEx and TCGA) comparing glioblastoma and low-grade glioma (LGG) tumors with normal tissues (Fig. 1B) and found that the RHOA, RHOC, DIAPH1, PFN1 and CFL1 genes were more highly expressed in GBM, while RHOB and MYPT1 were more highly expressed in LGG. Considering that the TP53 gene is the main gene responsible for the phenotypic differences between GBM and LGG tissues versus normal tissues (Fig. 1B), we mined this gene set in a cell line database (CCLE), comparing one p53-wild-type GBM cell line (U87-MG) with three p53-mutated GBM cell lines (T98G, U138-MG, U251-MG) and found that these five Rho pathway genes are expressed at similar levels in p53-proficient and p53-deficient GBM cells (Fig. 1C). However, the expression levels of each of the corresponding proteins differed among these four cell lines (Fig. 1D and S1A), and the T98G cell line was chosen and used hereafter as the p53-deficient model due to its higher protein levels of mutant p53 and phospho-p53 (Ser15) and lower p21 expression, in addition to its high expression and activity of RhoA and RhoB GTPases (Fig. 1D and S1B–D). Concurrently, the p53- wild-type cell model (U87-MG) exhibited a normal p21/p53 protein expression ratio at baseline and contained high levels of RhoA-GTP and RhoB-GTP (Fig. S1B–D). Kaplan–Meier survival analyses of patients with GBM based on RhoA, RhoB, RhoC, DIAPH1, PFN1, and MYPT1 gene expression (Fig. 1E) suggested that high expression of RHOA, RHOC, DIAPH1 and PFN1, low expression of RHOB and MYPT1, or both may be markers of poor prognosis in GBM patients. The effects of IR on the reduction in GBM cell survival, as investigated in U87-MG and T98G cells, showed higher resistance of p53-deficient cells to IR, with an ID_{50} approximately twice that found in wild-type p53 cells (Fig. S1E). The impact of Rho pathway modulation under the effects of IR was quantified in clonogenic survival assays of U87-MG and T98G cells by three different strategies (Fig. 1A): (1) inhibition of RhoA/B/C with C3 toxin (Fig. 1F, S2A–C); (2) knockdown of DIAPH1, PFN1, and MYPT1 (Fig. 1G–I and S2D–F); and (3) inhibition of actin polymerization with cytochalasin D (Fig. 1J and S2G). Overall, the results indicated that downregulation of the Rho pathway at these different levels reduced the survival of only p53-wild-type cells (Fig. 1F–H, J), while Rho pathway activation (through MYPT1 knockdown) promoted cell survival in response to 5 Gy of IR (Fig. 1I).

Downregulation of the Rho pathway increases DNA damage in a p53-dependent manner

Upregulated expression or overactivation of Rho pathway components plays essential roles in the malignant phenotype of GBM and resistance to IR, presumably driving the activation of DNA damage response and repair mechanisms. Thus, DNA strand break repair kinetics in U87-MG and T98G cells were analyzed by alkaline comet assays for up to 4 h after IR treatment (Fig. 2). Inhibition of Rho activity with C3 toxin caused accumulation of DNA damage in U87-MG cells (Fig. 2A, C), in contrast to the normal recovery of T98G cells (Fig. 2B, C). Similar results were obtained after knockdown of DIAPH1 (Fig. 2D, E, J) or PFN1 (Fig. 2F, G, J) in these cells. Conversely, MYPT1 knockdown led to higher resistance of both cell lines to IR, as indicated by the low levels of DNA fragmentation (Fig. 2H, I, J). The resistance phenotype of T98G cells to combined treatment with Rho pathway downregulation and IR was also observed after blockade of actin polymerization with cytochalasin D (Fig. 2K–M), which promoted DNA fragmentation persisting for up to 4 h only in U87-MG cells.

The formation of γH2AX(Ser139) foci is modulated by the Rho pathway in the wild-type p53 background

The formation of γH2AX foci in response to 5 Gy IR exposure, as an indicator of early DNA damage response (DDR) signaling, was strongly prevented by Rho inhibition in U87-MG cells (Fig. 3A, B), while it was weakly attenuated in the p53-mutated background (Fig. 3C, D). Similarly, DIAPH1 knockdown caused a decrease in γH2AX foci formation after IR in U87-MG cells (Fig. 3E, F) but not in T98G cells (Fig. 3G, H). In contrast, after MYPT1 knockdown, a high number of γH2AX foci per nucleus was maintained only in U87-MG cells, with the p53-wild-type background (Fig. 3E–H). However, cytochalasin D treatment diminished the number of γH2AX foci after IR in U87-MG cells (Fig. 3I, J) but not in T98G cells (Fig. 3K, L).

Modulation of Rho activity affects the NHEJ pathway in a p53-dependent manner and the HR pathway in a p53-independent manner

Quantification of NHEJ activity was performed by transfecting cells with a GFP reporter gene whose expression is dependent on the repair of a DSB in the vector mediated by the restriction enzyme I-SceI; if repair occurs by any type of NHEJ pathway, GFP is expressed, and the repair activity can be quantified by determining the number of GFP-positive cells (Fig. 4A). Under conditions of Rho inhibition, this functional assay showed that NHEJ repair was highly impaired in U87-MG cells (Fig. 4B) but not in T98G cells (Fig. 4C). These effects were reproduced by knockdown of DIAPH1 and reversed by knockdown of MYPT1 only in U87-MG cells

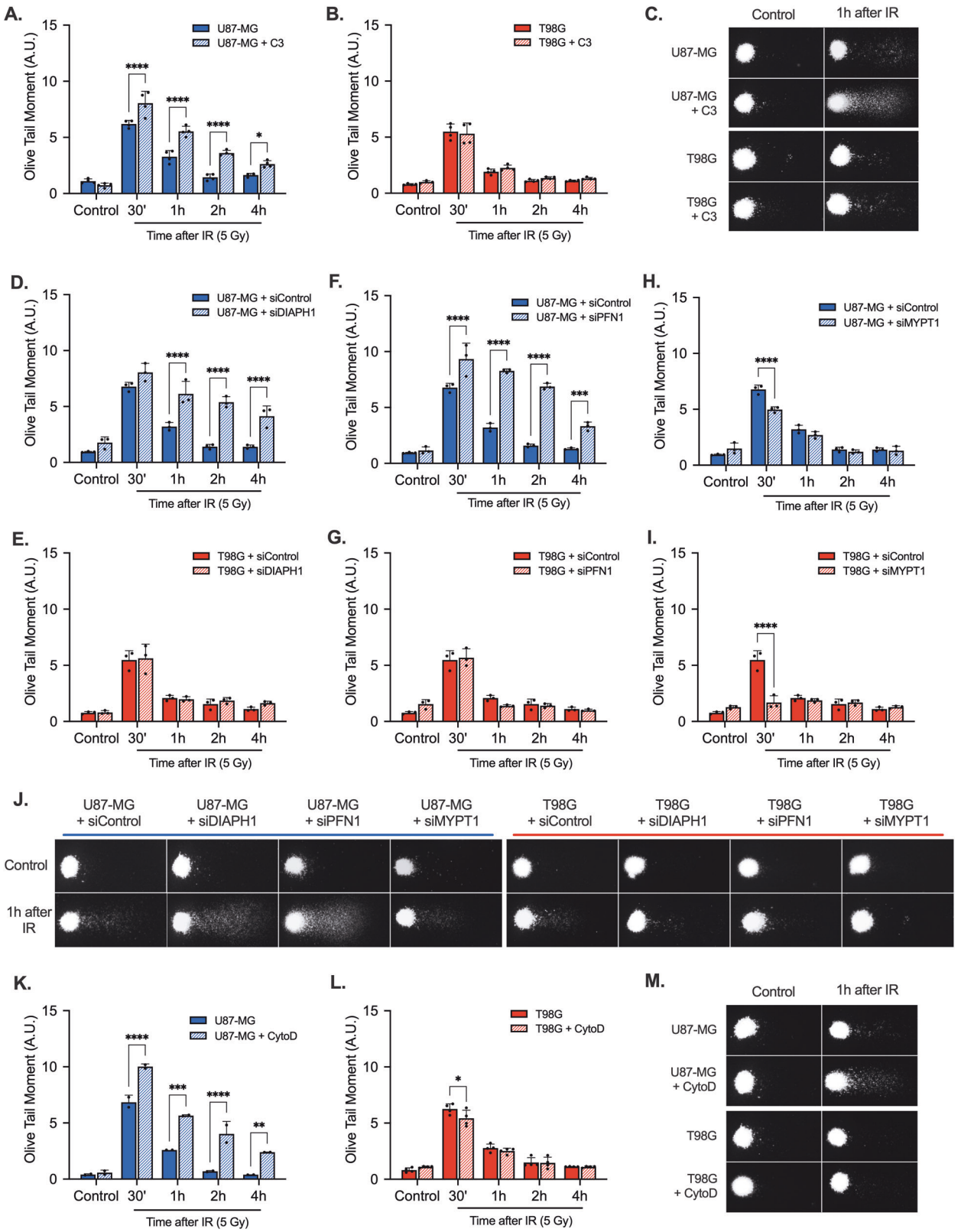

Fig. 2 Downregulation of the Rho pathway reduces the repair of DNA damage caused by IR in wild-type p53 glioma cells. Comet assays of U87-MG (**A**) and T98G (**B**) cells with Rho inhibition induced by C3 toxin treatment and IR-induced DNA damage; DNA repair is impaired by C3 toxin treatment in wild-type p53 cells but not in mutant p53 cells. Comet assays of GBM cells exposed to IR after knockdown of DIAPH1 (**D**, U87-MG and **E**, T98G) or PFN1 (**F**, U87-MG and **G**, T98G) indicate decreased DNA repair and persistent DNA fragmentation for up to 4 h after IR stress, but only in U87-MG cells. Conversely, MYPT1 knockdown (**H**, U87-MG and **I**) leads to higher resistance to IR in both cell lines, as indicated by the decreased DNA fragmentation after IR. Comet assays of U87-MG (**K**) and T98G (**L**) cells subjected to inhibition of F-actin polymerization with CytoD treatment show increased DNA fragmentation after IR stress only in wild-type p53 cells and not in T98G cells. Representative images of comet tail relative to the 1-h time point after IR (**C**, **J**, and **M**). The graphs show the mean ± SD of three or four independent experiments, with the averages of individual biological replicate dots from the analysis of DNA fragmentation in 100 independent nuclei by two-way ANOVA with Sidak's multiple comparison test.

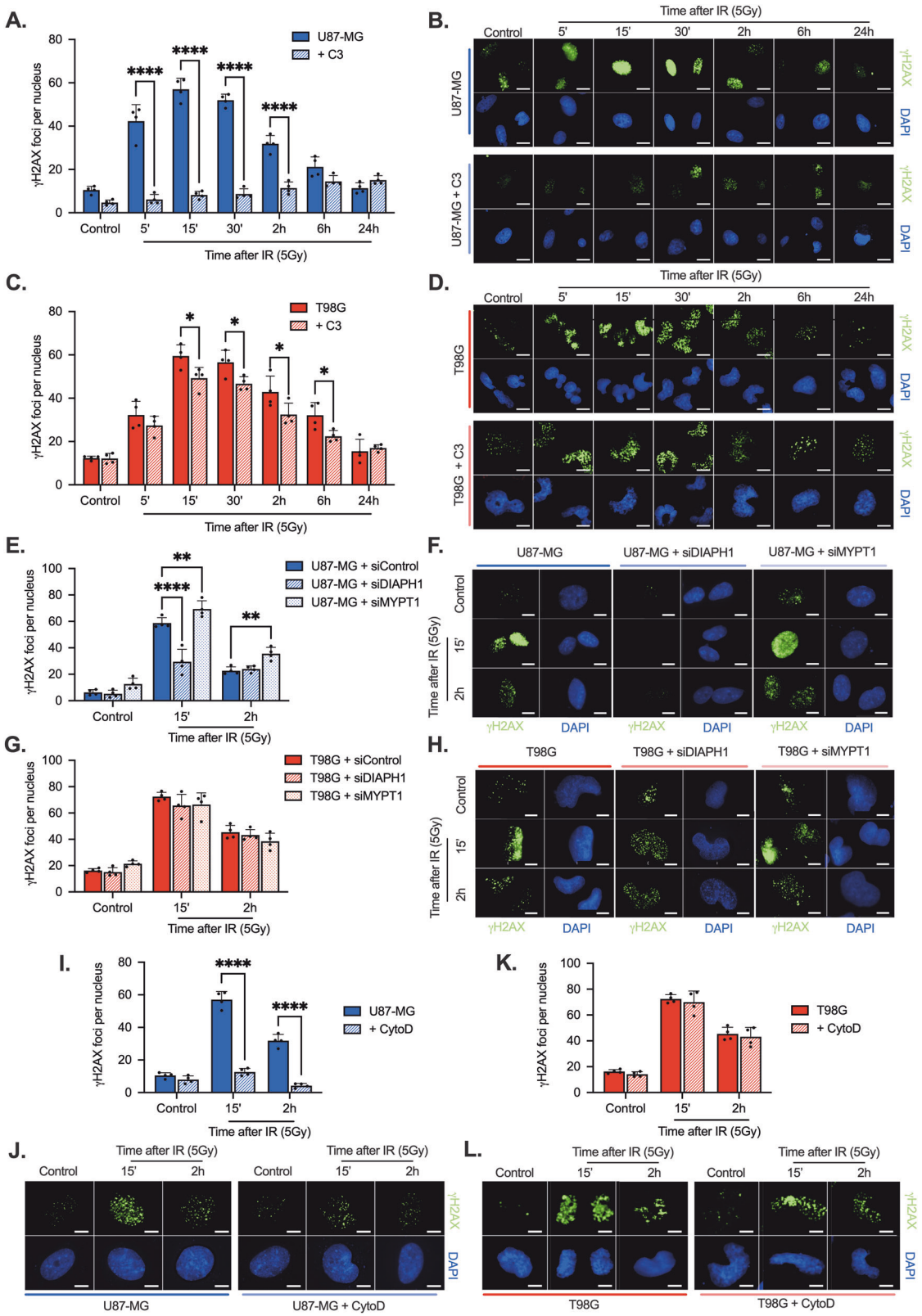

(Fig. 4D), while these changes did not occur in p53-deficient cells (Fig. 4E). In corroboration of the finding that NHEJ pathway function depends on Rho activity, Rho inhibition reduced the number of 53BP1 foci per nucleus in U87-MG cells (Fig. 4F, G) compared to T98G cells (Fig. 4H, I), again suggesting that 53BP1 recruitment to DNA damage sites is Rho-dependent only in p53-wild-type cells. DSB repair activity through the HR pathway was quantified by transfecting cells with an inactive GFP reporter gene, which is repaired by the HR machinery using a 3' inactive fragment of GFP (iGFP) located downstream of the reporter gene,

Fig. 3 Rho inhibition reduces γH2AX foci formation in response to IR stress in a p53-dependent manner. A–D After 5 Gy IR exposure, in U87-MG cells and T98G cells (respectively, **A**, **C** quantification of foci per nucleus; **B**, **D** representative immunofluorescence panel) previously subjected to C3 toxin treatment, DNA damage signaling through H2AX phosphorylation at the damage site is prevented by Rho inhibition, with a stronger effect in wild-type p53 cells. **E–H** Similar to C3 toxin treatment, knockdown of DIAPH1 decreases the formation of γH2AX foci in U87-MG cells, whereas MYPT1 silencing increases DNA damage signaling through H2AX phosphorylation, again observed only in wild-type p53 cells (respectively, **E**, **G** quantification of foci per nucleus; **F**, **H** representative immunofluorescence panel). **I–L** In U87-MG and T98G cells treated with Cyto D followed by 5 Gy IR exposure (**I**, **K** quantification of foci per nucleus; **J**, **L** representative immunofluorescence panel), F-actin depolymerization at the final stages of the Rho pathway causes a reduction in γH2AX foci formation only in U87-MG cells. Immunofluorescence images were acquired with a 63x objective; the scale bars indicate 10 μM. The graphs show the mean ± SD of three or four independent experiments, with the averages of individual replicate dots from the number of foci in 100 individual nuclei, as analyzed by two-way ANOVA with Sidak's multiple comparison test.

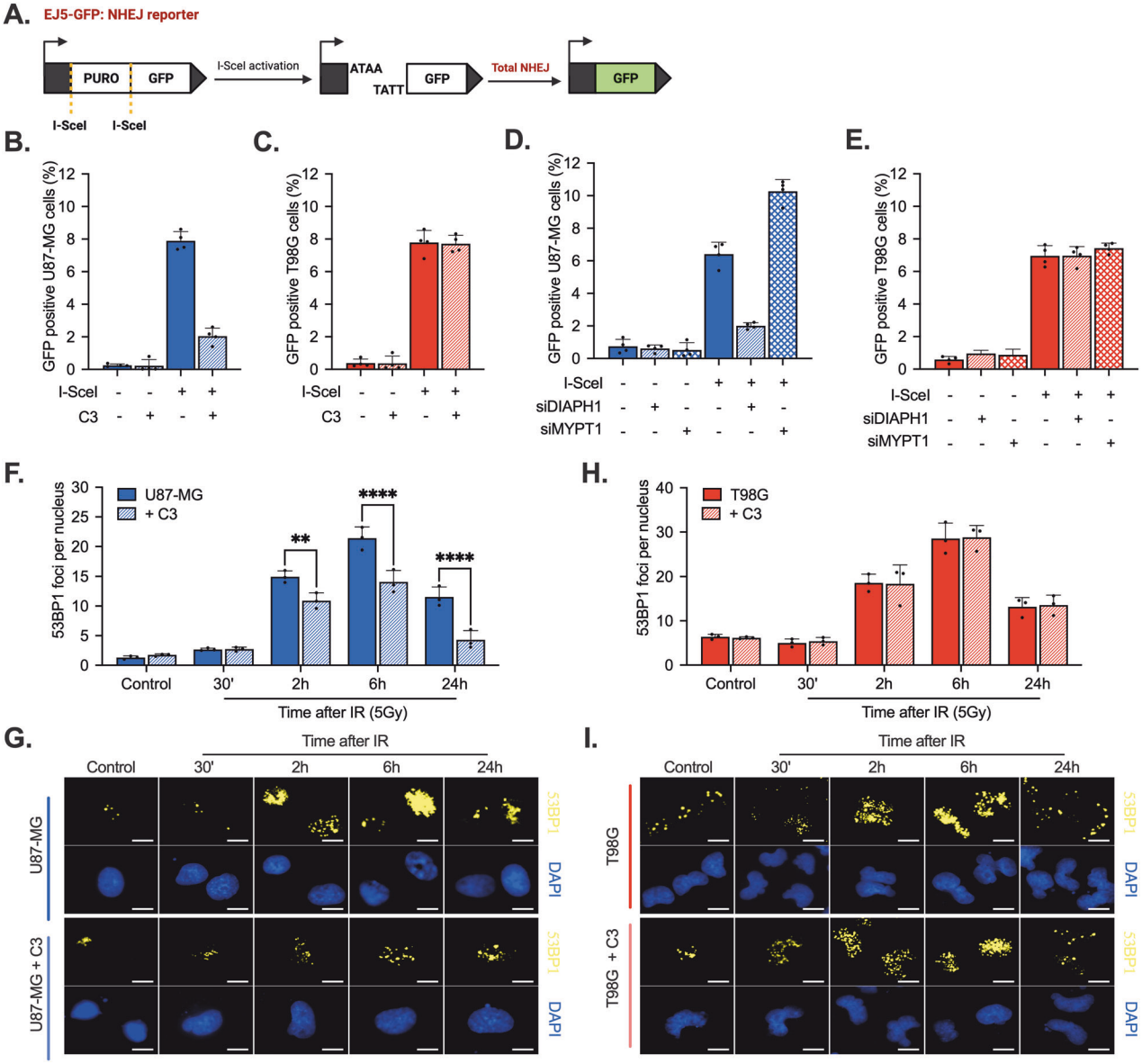

Fig. 4 The nonhomologous end-joining (NHEJ) repair pathway is targeted by Rho inhibition in wild-type p53 cells. A Schematic drawing of the EJ5-GFP vector used for quantification of DSB repair by NHEJ, created with BioRender.com. The vector contains the GFP gene truncated by a puromycin resistance gene, which is flanked by two I-SceI restriction sites. I-SceI expression promotes the generation of two breaks in the vector, and if repair occurs by any NHEJ pathway, GFP is expressed, and repair activity can be quantified by determining the number of GFP-positive cells. **B**, **C** NHEJ assays show that Rho inhibition by C3 toxin treatment strongly decreases repair in U87-MG cells (**B**) but not in T98G cells (**C**). Similarly, DIAPH1 knockdown (**D**) also decreases the NHEJ repair capacity, while MYPT1 knockdown enhances the NHEJ repair capacity (**E**). **F–I** 53BP1 foci formation in response to IR stress was analyzed in U87-MG (**F**, **G**) and T98G (**H**, **I**) cells with Rho inhibition induced by C3 toxin treatment. The kinetics of 53BP1 recruitment to DNA damage sites are slowed by Rho inhibition only in wild-type p53 cells (**F**, **H** quantification of foci per nucleus; **G**, **I** representative immunofluorescence panel). Immunofluorescence images were acquired with a 63x objective; the scale bars indicate 10 μM. The graphs show the mean ± SD of three or four independent experiments, with the averages of individual replicate dots from the GFP signal of 2000 cells, as analyzed by one-way ANOVA in NHEJ assays, or the number of foci in 100 individual nuclei, as analyzed by two-way ANOVA with Sidak's multiple comparison test in the 53BP1 foci assay.

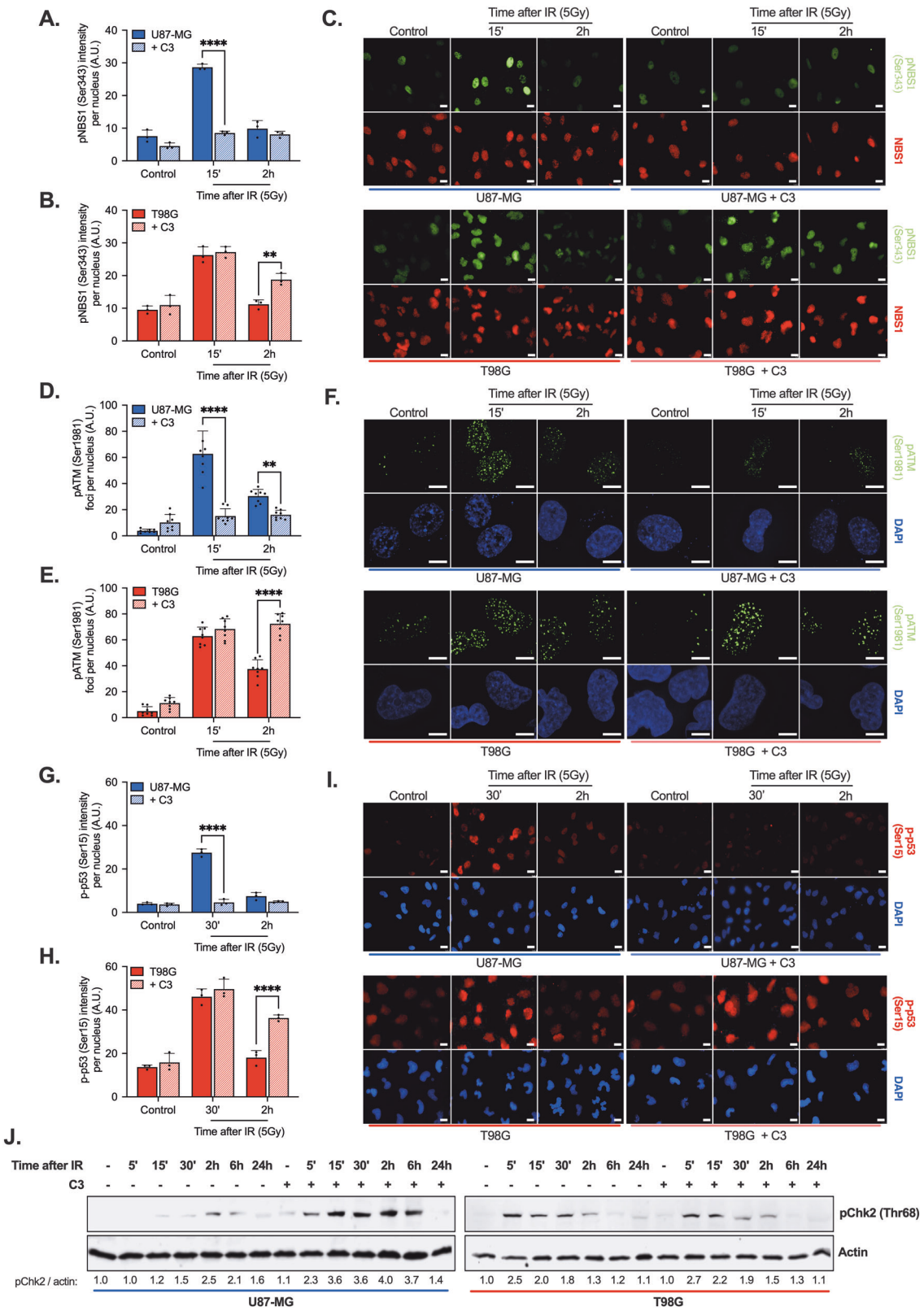

as a template (Fig. S3A). In the presence of Rho inhibition or knockdown of DIAPH1, HR repair was impaired in T98G cells, whereas MYPT1 knockdown enhanced HR repair, as determined by the increase in the number of GFP-positive cells (Fig. S3B). Unlike the NHEJ pathway, the HR pathway was affected by modulation of the Rho pathway only in p53-mutant cells, since no viable DR-GFP U87-MG clones were isolated. Analysis of pBRCA1 foci in response to IR as an early indicator of HR showed that treatment with C3 toxin almost completely abolished both the recruitment of pBRAC1 to DSB sites and the phosphorylation of BRCA1 (Ser1524) in U87-MG cells but not in T98G cells (Fig. S3C). Furthermore, analysis of Rad51 protein expression as a late

Fig. 5 Inhibition of the Rho pathway attenuates DDR signaling and thereafter suppresses DSB repair in wild-type p53 cells. A–C Phosphorylation of NBS1 (Ser343) is blocked by Rho inhibition in U87-MG cells in response to IR stress (**A**), and in T98G cells, C3 toxin treatment does not prevent NBS1 phosphorylation but maintains it at a high level, even 2 h after IR (**B**). Representative panels show pNBS1 in green, NBS1 in red and DAPI in blue (**C**). **D–F** pATM (Ser1981) foci formation in response to IR stress in U87-MG (**D**) and T98G cells (**E**) under Rho inhibition prevents IR-induced ATM phosphorylation in U87-MG cells, while in T98G cells, Rho inhibition leads to persistent phosphorylation of ATM 2 h after IR. Representative panels show pATM in green and DAPI in blue (**F**). **G–I** IR-induced p53 phosphorylation (Ser15) was inhibited by C3 toxin treatment in U87-MG cells (**G**) but not in mutant p53 cells (T98G), where p53 shows high levels of phosphorylation under stress-free conditions, which seem unaffected by Rho inhibition (**H**). Representative panels show p-p53 (Ser15) in red and DAPI in blue (**I**). Immunofluorescence images were acquired with a 63x objective; the scale bars indicate 10 μM. The graphs show the mean ± SD of three independent experiments for NBS1 and p53 phosphorylation analysis or eight for ATM phosphorylation analysis, with the averages of individual replicate dots from the number of foci in 100 individual nuclei, as analyzed by two-way ANOVA with Sidak's multiple comparison test. **J** Rho inhibition increases the phosphorylation of Chk2 (Thr68) in response to IR over time in U87-MG cells (left panel) but not in T98G cells, in which Chk2 phosphorylation remains unaffected (right panel) by C3 toxin treatment. The immunoblots are representative of three independent experiments. The replicate blots are available in the Original Data File.

indicator of HR repair showed that Rho inhibition increased Rad51 expression up to 6 h after IR treatment in both cell lines, that is, independent of the p53 status (Fig. S3D).

The DNA damage response pathway is sensitive to Rho inhibition in the p53-wild-type background

Changes in classical protein markers acting early or late in the DDR pathway in response to IR stress were assessed (Fig. 5). Recruitment and phosphorylation of NBS1 (Ser343) at the sites of IR-induced DSBs were impaired by C3 toxin treatment in U87-MG cells (Fig. 5A, C) but remained robust in T98G cells (Fig. 5B, C). These results were consistent with the ATM activity detected in the p53-deficient background in comparison to the p53-wild-type background (Fig. 5D–F). The formation of pATM (Ser1981) foci showed that Rho inhibition prevented IR-induced ATM phosphorylation in U87-MG cells (Fig. 5D, F), with no such effect in T98G cells (Fig. 5E, F). The ATM activity also reflected IR-induced p53 (Ser15) phosphorylation in U87-MG and T98G cells (Fig. 5G–I): in p53-wild-type cells, Rho inhibition prevented p53 phosphorylation, while p53-mutant cells exhibited high levels of phospho-p53 (Ser15) that were further increased by treatment with C3 toxin. On the other hand, the kinetic profile of Chk2 (Thr68) phosphorylation in response to IR differed markedly between these cell lines (Fig. 5J, S4A): Rho inhibition promoted an increase in Chk2 (Thr68) phosphorylation in U87-MG cells after IR stress but had no such effect on T98G cells. This unexpected IR-induced Chk2 activation seems to be dependent on p53 transcriptional activity but independent of Rho activity and possibly caused by the higher basal level of phospho-p53 (Ser15) in T98G cells, which can modulate the phospho-Chk2 (Thr68) level [31]. The schematic summary showing the modulation of DDR and DSB repair mechanisms in GBM cells with different p53 status (wild-type versus mutated) in the presence or absence of an active Rho pathway confirms that attenuation of Rho pathway activity decreases DDR signaling and, thereafter, DSB repair in wild-type p53 cells (Fig. S4B). All phenotypes found in U87-MG cells were reversed in the mutant p53 background, except for HR repair, which was impaired by Rho downregulation in T98G cells.

The modulation of p53 expression/activity affects the Rho-dependent DDR and repair pathways

As proof of concept, the interdependence between the Rho and p53 pathways was evaluated (Fig. 6). The maximum efficiency of p53 knockdown occurred 72 h after siRNA transfection in U87-MG cells: p53 protein expression was reduced by 90%, which in turn decreased p21 expression by 50% and the phospho-CFL1 (Ser3) protein level by 20% (Fig. 6A and S5A). The IR dose-dependent reduction in the viability of U87-MG cells was enhanced by Rho inhibition, but viability was significantly restored by p53 knockdown and independent of C3 toxin treatment (Fig. S5B). Comet assays of U87MG cells with IR-induced DNA damage showed that p53 knockdown did not interfere with DSB repair, while Rho inhibition increased this damage (Fig. 6B, C) in the presence of wild-type p53, although this effect was abolished by p53 knockdown. In confirmation of these results, p53 knockdown in p53-mutant cells increased DNA damage independent of Rho activity (Fig. S5C). The ability of U87-MG cells to repair IR-induced damage is correlated with their capacity to sense the rapid increase in DSB sites and directly linked to Rho inhibition and p53 knockdown. The blockade of H2AX phosphorylation and/or γH2AX foci formation at damage sites promoted by C3 toxin treatment was largely prevented by previous p53 knockdown (Fig. 6D, E). Furthermore, p53 knockdown elicited reductions in RhoA and RhoB activity without affecting their protein levels (Fig. 6F and S5D), which caused disruption of the stress fiber network (Fig. S5E), suggesting interdependence between the Rho and p53 pathways. In addition, similar data were obtained in two different p53-wild-type GBM cell lines (A172 and U343-MG), where Rho inhibition also increased sensitivity to IR and impaired IR-induced DNA break repair (Fig. S5F, G). To exclude the possible Rho specificity of T98G cells, we carried out analysis of the mutation profiles of the three GBM cell lines (T98G, U138-MG, and U251-MG) with mutant p53 chosen for this work. The Venn diagram shows that among the hundreds of mutations present in these cells, only one was common to all cell lines: TP53 gene mutation (Fig. 6G). These mutant cells exhibit loss-of-function (LoF) of p53 since they harbor point mutations in the DNA-binding domain (DBD), leading to the loss of canonical transcriptional activity, although U138-MG and U251-MG cells harbor the same missense mutation (R175H) in the p53 protein, unlike T98G cells (M237I). However, similar to that of T98G cells, the survival of U138-MG and U251-MG cells in response to IR was not affected by Rho inhibition (Fig. 6H) or the repair of IR-induced DSBs (Fig. 6I, J). To restore the phenotype of p53mutant cells to a p53-wild-type phenotype, p53 transcriptional activation assays were performed in U138-MG and U251-MG cells treated with PRIMA-1. A promoter activated by wild-type p53 fused to a luciferase reporter gene was transiently transfected into both cell lines, and the cells were subsequently treated with 50 μM PRIMA-1 for 24 h, which was able to restore the transcriptional capacity of p53 in U138-MG cells but not in U251-MG cells (Fig. 6K) or in T98G cells [32]. Considering this finding, we performed comet assays in U138-MG cells subjected to IR-induced DNA damage after p53 reactivation with PRIMA-1 and/or Rho inhibition (Fig. 6L, M). Restoration of p53 activity by PRIMA-1 sensitized U138-MG cells to Rho inhibition in response to IR and resulted in a wild-type phenotype in p53-mutant cells. Consistent with these results, PRIMA-1 treatment did not change the p53 protein level; however, interestingly, it elevated the p21 and pCFL1 levels (Fig. S5H). Overall, these results are consistent with those previously found after Rho pathway inhibition in U87-MG cells.

Rho activity regulates p53 wild-type localization and transcriptional activity through G-actin availability

In U87-MG cells, either inhibition of Rho activity by C3 toxin treatment or F-actin polymerization using cytochalasin D induced

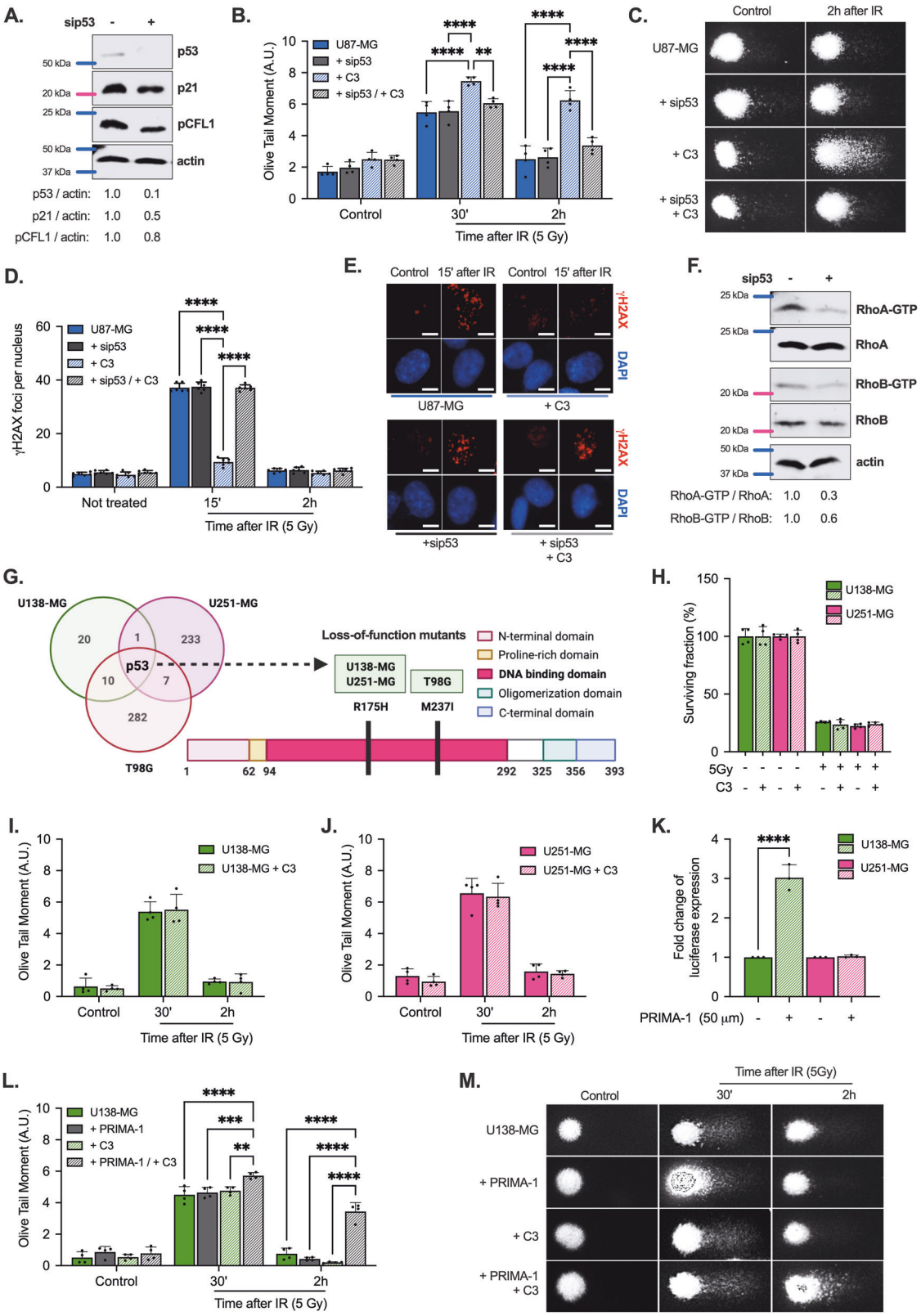

p21 protein expression, whereas the p53 level remained unchanged (Fig. 7A and S6A). Both inhibitory treatments increased p53 transcriptional activity despite IR stress exposure (Fig. 7B, C), suggesting the nuclear localization of p53 associated with low actin polymerization. To investigate this correlation, we used another strategy to modulate Rho pathway activity through the starvation of U87-MG cells in serum-free medium (SFM) with subsequent addition of high levels of serum (Fig. S6B). Starvation in SFM for 48 h decreased RhoA and RhoB activity, as well as CFL1 phosphorylation, while stimulation with a 30% FBS pulse for 30 min strongly increased

Fig. 6 Modulation of p53 expression and activity interferes with the Rho pathway in GBM cells in response to IR. A At 72 h, p53 knockdown decreases p53 expression by 90%, p21 expression by 50% and phosphorylation of CFL1 (Ser3) by 20% in U87-MG cells. The immunoblots are representative of three independent experiments. The replicate blots are available in the Original Data File. **B** Rho inhibition by C3 toxin treatment increases IR-induced DNA damage in U87-MG cells, and this increase is reversed by p53 knockdown. Representative panels showing time points in the comet assay relative to the 2 h time point after IR (**C**). The graphs show the mean ± SD of four independent experiments, with the averages of the individual replicate dots from the DNA fragmentation results in 100 independent nuclei. **D** p53 knockdown prevents the blockade of H2AX phosphorylation after IR stress promoted by Rho inhibition in U87-MG cells. Representative immunofluorescence panels showing γH2AX in red and DAPI in blue (**E**). Immunofluorescence images were acquired with a 63x objective; the scale bars indicate 10 μM. The graphs show the mean ± SD of five independent experiments, with the averages of the individual replicate dots from the number of γH2AX foci in 100 individual nuclei, as analyzed by two-way ANOVA with Sidak's multiple comparison test. **F** In U87-MG cells, p53 knockdown promotes a decrease in the activity of both RhoA and RhoB. **G** Analysis of the mutation profiles of three GBM cell lines harboring mutant p53 shows that among the hundreds of existing mutations, the p53 gene mutation is the only one in common (Venn diagram). These mutant cells harbor point mutations in the DNA-binding domain leading to loss of the canonical transcriptional activity of p53, i.e., loss-of-function (LoF) mutations. **H** The survival of U138-MG and U251-MG cells in response to IR is not affected by C3 toxin treatment. The graphs show the mean ± SD of four independent experiments, with the averages of individual biological replicate dots from two colony wells, as analyzed by two-way ANOVA with Tukey's multiple comparison test. Similar to the observations in T98G cells, Rho inhibition in U138-MG (**I**) and U251-MG cells (**J**) exposed to IR stress does not affect DNA repair. **K** Treatment with 50 μM PRIMA-1 for 24 h restores the transcriptional activity of p53 in U138-MG cells but not in U251-MG cells. **L** U138-MG cells, previously subjected to reactivation of p53 activity by treatment with PRIMA-1, were treated with C3 toxin and subsequently exposed to IR stress. Reactivation of p53 sensitizes U138-MG cells to Rho inhibition in response to IR, driving cells with the original mutant p53 status to acquire a phenotype similar to that of wild-type p53 cells. Representative panels of the comet assay relative to U138-MG cells treated with PRIMA-1, C3 toxin and IR (**M**). The graphs show the mean ± SD of four independent experiments, with averages of the individual replicate dots from the DNA fragmentation results in 100 independent nuclei, as analyzed by two-way ANOVA with Sidak's multiple comparison test.

these levels (Fig. 7D and S6C). Using the same strategy, we monitored p53 localization in U87-MG cells for up to 6 h after the 30% FBS pulse, quantifying the percentage of nuclear p53 by staining nuclei with DAPI and using high-throughput acquisition software (Fig. 7E, F). In exponentially growing cells, p53 was almost equally distributed in the cytoplasm and nucleus, while after FBS starvation, p53 localization was mostly nuclear. Immediately and for up to 30 min after the 30% FBS pulse, p53 localization was mostly cytoplasmic, but p53 gradually accumulated in the nucleus after that point, with a 1:1 nuclear:cytoplasmic ratio observed ~6 h after FBS stimulation (Fig. 7E, F). More importantly, the preferential cytoplasmic localization of p53 resulted in low levels of p21 protein expression (Fig. 7G and S6D). As p53 entered the nucleus, the levels of p21 increased, consistent with the augmented activity of the Rho pathway, as determined by the phosphorylation of CFL1 (Fig. 7G and S6E). Our results confirm those previously proposed by others [33] that the higher Rho activity is, the greater the polymerization of F-actin and the cytoplasmic retention of p53, while in contrast, the potent and rapid inhibition of actin polymerization by cytochalasin D promoted rapid nuclear translocation of p53, correlated with the availability of cytoplasmic G-actin (Fig. 7H, I). These findings indicate that Rho activity regulates the localization and transcriptional activity of p53, as monitored by the pCFL1 and p21 levels, respectively (Fig. 7J and S6E). The percentage of nuclear p53 in U87-MG cells after IR stress was also examined, since actin polymerization and nuclear p53 localization are triggered by DNA damage [33]. Therefore, we downregulated the Rho pathway by C3 toxin treatment, cytochalasin D treatment, or serum starvation with or without subsequent FBS stimulation. IR induced p53 translocation to the nucleus, which was strongly enhanced by inhibition of Rho activity or actin polymerization; however, this effect was strongly mitigated through activation of the Rho pathway (Fig. 7K).

IR-resistant U87-MG cells show increased viability and expression/activity of Rho, p53, DDR, NHEJ and HRR pathway components, a resistance phenotype reversed by Rho inhibition in a manner dependent on wild-type p53

The interdependence between the Rho and p53 pathways versus the sensitivity/resistance of gliomas to IR was tested. As proof of concept, we established a protocol for the generation of IR-resistant clones, as follows: U87-MG cells were seeded and grown to 70% confluence in several culture bottles, and each bottle was subjected to cycles of different doses of IR to obtain resistant clones. The clone named IR R-1 was first exposed to once-weekly cycles of 2 Gy IR for 4 weeks. Then, for 3 weeks, the cells were subjected to two cycles of 2 Gy IR per week. Next, the cells were exposed to two cycles of 5 Gy IR per week for 2 weeks. Finally, the cells were irradiated with 10 Gy weekly for 2 weeks, reaching the final cumulative IR dose of 60 Gy (Fig. 8A). In comparison to U87-MG cells, which naturally exhibit IR resistance, IR R-1 clones exposed to increasing doses of IR displayed higher resistance in viability assays, as evidenced by the increase in the ID_{50} from 8 Gy to 34 Gy (Fig. 8B). IR R-1 cells exhibited markedly distinct F-actin structures, increased stress fiber formation and actin protrusions compared to U87-MG cells, which is suggestive of increased Rho pathway activity (Fig. 8C). Immunoblotting and pulldown assays confirmed the increased expression/activity of Rho pathway components (RhoA, pCFL1 and PFN1) in IR R-1 clones in comparison to U87-MG cells (Fig. 8D and S7A). More importantly, IR R-1 clones exhibited higher basal levels of DNA damage and repair proteins in the p53 (low p21 expression), DDR (γH2AX and pChk2), NHEJ (Ku80), and HRR (Rad51) pathways than did U87-MG cells (Fig. 8E and S7B). Next, we showed that Rho inhibition by C3 toxin (Fig. 8F and S7C) or cytochalasin D (Fig. S7D) treatment in IR R-1 clones reversed IR resistance to the level observed in U87-MG cells. The viability of U87-MG and IR R-1 cells after IR stress and under Rho inhibition is linked to the formation of γH2AX foci: IR-resistant clones showed more γH2AX foci under stress-free conditions than did U87-MG cells, but this DNA damage sensitivity was rapidly reversed after IR and was still decreased by C3 toxin treatment in parental cells but not in IR R-1 clones (Fig. 8G and S7E). Finally, cell viability assays performed in U87-MG and IR R-1 clones with Rho inhibition associated with or independent of p53 knockdown showed that IR R-1 clones maintained their resistance to IR even in the setting of p53 knockdown when compared to U87-MG cells; however, Rho pathway inhibition with C3 toxin reversed the IR-R-1 clones' resistance to IR, and this effect was abolished by p53 knockdown (Fig. 8H), again confirming the interdependence between the Rho and p53 pathways in mediating glioblastoma resistance traits.

A 3D spheroid model of U87-MG cells (Fig. S8A, B) was used to investigate the proposed molecular mechanism in this tumor-like structure through two distinct approaches. In the first experiment, preformed spheroids were treated with cytochalasin D and IR (Fig. S8C). Depolymerization of the actin cytoskeleton strongly increased the spheroid size in a dose-dependent manner, and this effect was subtly reduced by IR, especially at high cytochalasin concentrations (Fig. S8D, E). This size increase did not seem to be

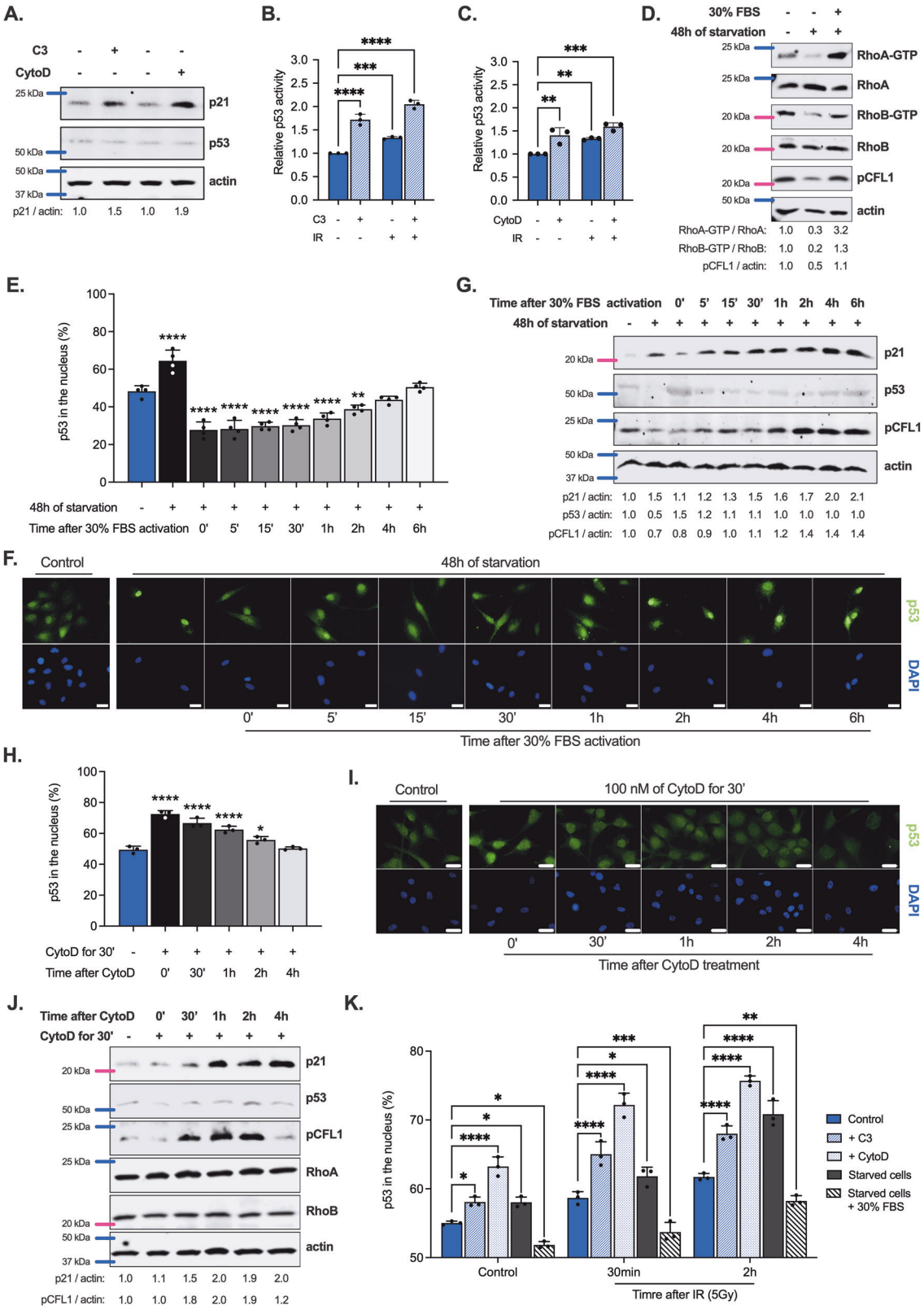

caused by cell proliferation, growth, death, or viability (Fig. S8F, G) and was more likely due to the weakening of the cell–matrix and/or cell–cell interactions in the spheroid model. An adapted comet assay established in our laboratory to analyze DNA strand breaks in spheroids proved the proposed mechanistic model, since cytochalasin D treatment also maintained high levels of DNA damage hours after irradiation of the spheroid model established with p53-wild-type cells (Fig. S8H). Next, evaluation of de novo spheroid formation (Fig. S8I, J) showed that pretreatment with cytochalasin D produced looser spheroids, and this morphology

Fig. 7 Attenuation of the Rho pathway interferes with the nuclear localization and transcriptional activity of p53. A Either Rho inhibition by C3 toxin or F-actin depolymerization by CytoD increases p21 but not p53 expression in U87-MG cells and increases the transcriptional activity of wild-type p53 (**B** and **C**, respectively) after IR stress. **D** Serum starvation decreases RhoA and RhoB activity, as well as phosphorylation of CFL1 (Ser3), in U87-MG cells, while activation with 30% FBS strongly increases RhoA and RhoB activity and CFL1 phosphorylation. **E** The percentage of nuclear p53 in U87-MG cells is increased by serum starvation but subsequently diminished after Rho activation induced by pulsing with 30% FBS for 30 min. Data at all time points were collected after switching the 30% FBS medium to regular 10% FBS medium. Representative panel of immunofluorescence images used for quantitation of p53 localization after inhibition and reactivation of the Rho pathway, showing DAPI in blue and p53 in green (**F**). **G** Rho inhibition through serum-free starvation increases nuclear p53 levels, causing increased p21 expression, which is rapidly diminished by Rho activation induced by FBS addition. Following Rho activation, which can be chased by increasing pCFL1 levels, the p53 level in the nucleus increases, promoting a gradual increase in p21 expression. **H** Inhibition of the Rho pathway by CytoD treatment promotes nuclear p53 localization in U87-MG cells, which returns to basal conditions as F-actin polymerization reverses the CytoD effects over time. Representative panel of immunofluorescence images used for quantitation of p53 localization after inhibition and reactivation of the Rho pathway, showing DAPI in blue and p53 in green (**I**). **J** Immunoblot analysis showing that F-actin depolymerization by CytoD treatment promotes CFL1 phosphorylation and increases p21 expression, which are due to p53 translocation to the nucleus, in U87-MG cells. **K** Rho inhibition by C3 toxin treatment, CytoD treatment or serum starvation induces p53 translocation to the nucleus in U87-MG cells, which is enhanced by IR stress. Subsequent Rho activation with a pulse of 30% FBS for 30 min reduces the percentage of nuclear p53, but nuclear translocation of p53 is stimulated after IR-promoted DNA damage. The immunoblots are representative of three independent experiments. The replicate blots are available in the Original Data File. Immunofluorescence images were acquired with a 20x objective in a high-throughput image acquisition system, and the scale bars represent 10 μM. The graphs show the mean ± SD of three independent experiments, with the averages of individual replicate dots from at least 2000 nuclei per condition, as analyzed in StrataQuest software by two-way ANOVA with Sidak's multiple comparison test.

was modulated by IR treatment, again in a dose-dependent manner, as high doses of IR slightly decreased the size of de novo spheroids. In the second approach, Rho pathway activity was modulated in cells prior to spheroid formation (Fig. S8K); intriguingly, all of the tested modulations promoted the enlargement of spheroids– except for transfection of siMYPT1, which exhibited the opposite effect, consistent with Rho pathway activation (Fig. S8L, M)—and was capable of maintaining high levels of strand breaks at 2 h after IR, as measured by comet assays (Fig. S8N). These data can greatly improve the clinical relevance of the mechanism proposed here, thus opening prospective avenues for new preclinical and clinical studies.

DISCUSSION

Several mechanisms of GBM radioresistance have been identified, but these have not yet resulted in the development of effective means to sensitize these tumors and increase the efficiency of radiotherapy [7]. In this study, we propose a novel mechanism by which the Rho pathway and actin cytoskeleton act cooperatively with wild-type p53 in the repair of IR-induced DNA damage and promote GBM resistance (Fig. 8I). Our data reveal that Rho pathway activation enhances F-actin polymerization, which decreases G-actin-dependent p53 nuclear translocation and transcriptional activity, especially in the setting of genomic instability caused by IR stress. Unpolymerized cytoplasmic G-actin binds to p53 to promote its nuclear import and transcriptional activity according to the demand for nuclear p53 in the cellular response to DNA damage processing [33–35]. Furthermore, the reduction in p53 transcriptional activity promotes negative feedback that attenuates Rho activity, probably through modulation of the expression of Rho GEFs and GAPs, some of which are transcribed by p53, as well as the expression of RhoA and RhoC themselves [23, 36, 37]. The Rho-specific GAPs ARHGAP30 and ARHGAP11 were already shown to bind to wild-type p53 and promote its stabilization and activation [38].

Modulation of p53 activity affects DNA repair signaling pathways, such as the DDR and NHEJ pathways, which contribute to the acquisition of an IR-resistant phenotype. Our data extensively show that the Rho pathway and F-actin dynamics act in response to IR-induced stress in wild-type p53 GBM cells. Works from different laboratories have demonstrated that high activity of Rho GTPases, especially RhoA, is directly linked to high levels of DNA damage signaling and repair [11, 13, 15–18], but only now have we delineated the interdependency of Rho activity, actin polymerization, and p53 localization and activation for proper DDR signaling and DNA repair. We demonstrated that Rho pathway inhibition strongly decreases p53-dependent activation of DDR proteins, such as ATM, NBS1 and γH2AX. Regarding Chk2, a recent study revealed that Chk2 interacts with MYPT1, promoting its phosphorylation at Ser507 and chromosome maturation during mitosis [39]. Rho inhibition promotes an increase in MYPT1 activity, which could directly affect Chk2 (Thr68) phosphorylation. Considering the cell cycle-dependent processes, Chk2 can be phosphorylated independently of ATM by DNA-PK during the G2/M phase of the cell cycle [40]. To our knowledge, there is no report relating Rho GTPases to DNA-PK activity; however, it is known that ATM and DNA-PK reciprocally downregulate each other [41], suggesting that Rho inhibition decreases ATM activation and consequently increases DNA-PK activity, promoting wild-type p53-dependent Chk2 phosphorylation.

The NHEJ pathway was also affected by Rho pathway inhibition in wild-type p53 cells. These data are consistent with the DDR analysis of 53BP1 foci formation and suggest that Rho, together with p53, regulates DDR signaling, consequently affecting NHEJ repair [42]. Regarding HR repair, the mechanism appears to be independent of wild-type p53 and DDR signaling, since Rho inhibition does not affect BRCA1 phosphorylation (an early marker for HR repair) but increases Rad51 expression instead. This process seems to occur in the late steps of DSB repair through different processes, such as nuclear actin-mediated chromatin organization and relocation [43, 44].

Although the remarkable mechanism revealed herein is not active in p53-mutant cells, pharmacological p53 reactivation restores the Rho inhibition-induced sensitivity of glioma cells to IR. In fact, PRIMA-1 and PRIMA-1^{MET} (or APR-246) have been tested in several phase I/II clinical trials [45–47]. The safety and antitumor roles of APR-246 were already investigated in a phase I/IIa clinical trial of patients with leukemia, lymphoma or prostate cancer and presented a favorable toxicity profile in patients with p53 mutation, while no clinical response was observed in patients with wild-type p53, according to the predefined response criteria [47, 48], which nicely corroborates the mechanism proposed here and its relevance for future clinical approaches.

The most striking finding of this study is the possibility of reversing the IR-resistant phenotype of GBM cells through inhibition of either Rho pathway activity or F-actin polymerization, or even both, to promote increased radiation sensitivity and reduced repair of IR-damaged DNA with consequent accelerated cell death and tumor regression. In addition to the increases in the DDR and DNA repair, IR-resistant cells also display enhanced Rho pathway activity and F-actin polymerization, showing that the Rho

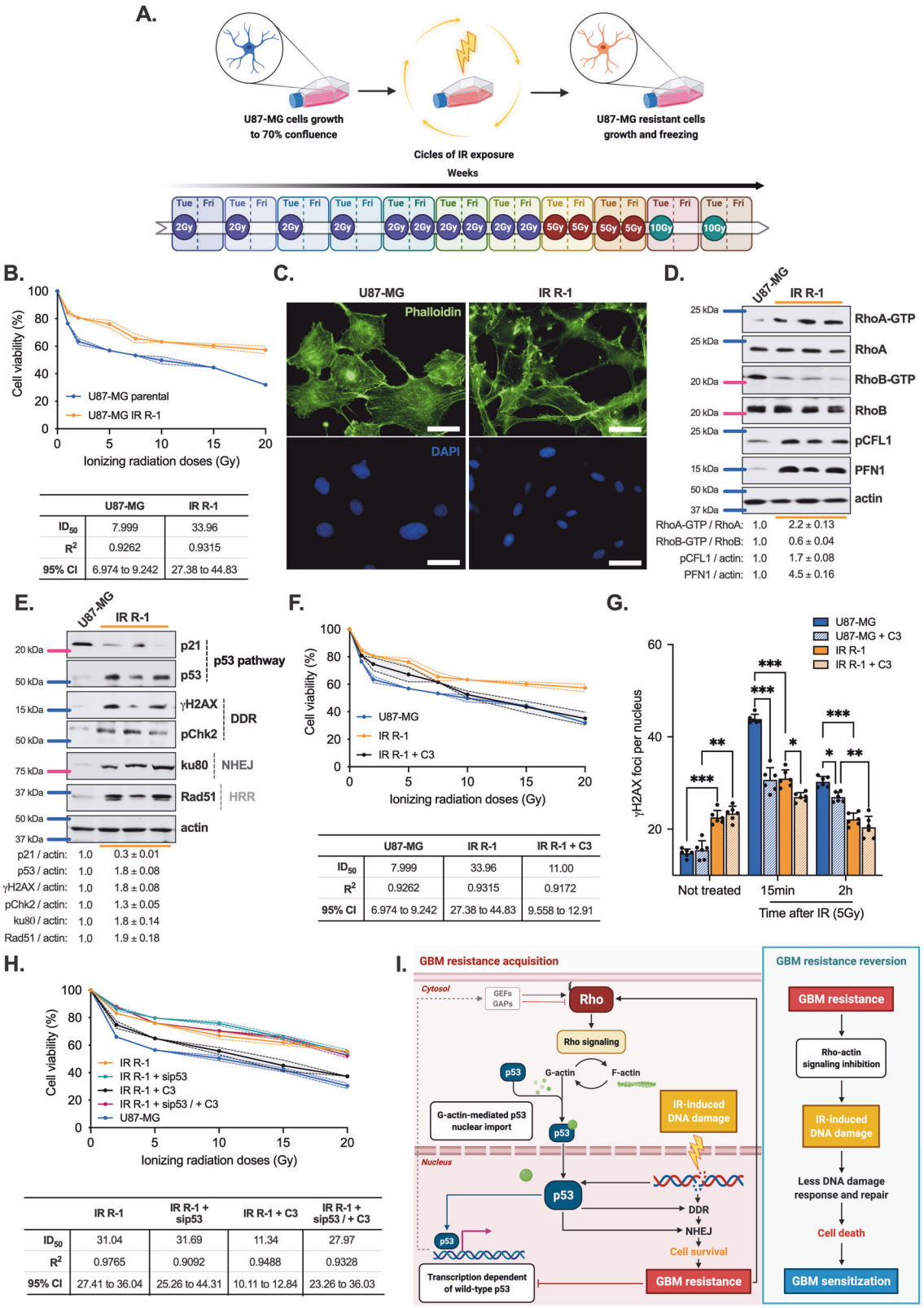

pathway is a major player in the acquisition of resistance. As outcomes, two regulatory aspects stand out: both enhanced activity of RhoA, which is generally described as an oncogene, and diminished RhoB activity, suggesting a tumor suppressor role [49–51], are features of IR-resistant cells and intimately related to the survival of GBM patients (Fig. 1F). These data can be used as preliminary and initial evidence for the events that would occur in recurrent tumors treated with a combination of radiation and actin drugs. In conclusion, our data shed light on the Rho pathway and actin cytoskeleton dynamics as promising targets for the

Fig. 8 Radioresistance of GBM cell clones can be modulated via the Rho pathway. A Flowchart of the protocol for generating IR-resistant U87MG clones over eleven consecutive weeks until the final cumulative dose of 60 Gy was reached. **B** IR R-1 clones display higher resistance and viability than parental U87-MG cells 72 h after exposure to increasing doses of IR. **C** IR R-1 cells exhibit distinct F-actin structures, with increased stress fiber formation and actin protrusions (F-actin (labeled with Alexa Fluor 488-phalloidin) in green and DAPI in blue). **D** IR R-1 cells exhibit increased Rho pathway activity (RhoA-GTP, pCFL1, and PFN1) compared to U87-MG cells, as shown by immunoblot analysis and pulldown assays. On the other hand, RhoB activity is diminished in IR R-1 cells. **E** Proteins related to distinct DNA damage signaling pathways were analyzed by immunoblotting as follows: (i) p53 pathway, (ii) DDR pathway, (iii) NHEJ repair, and (iv) HR repair. IR R-1 cells show increased expression of p53 associated with lower expression of p21, increased levels of H2AX and Chk2 phosphorylation, and increased levels of NHEJ and HR proteins (Ku80 and Rad51, respectively) compared to those in U87-MG cells. **F** C3 toxin treatment reverses IR resistance in IR R-1 cells, since the viability of the IR-resistant clones under Rho inhibition is reduced almost to the level in parental U87-MG cells, as determined by the IC_{50} values. **G** IR R-1 cells show high numbers of γH2AX foci under stress-free conditions; however, these cells show lower numbers of γH2AX foci after IR, and these numbers are slightly decreased by C3 toxin treatment. **H** p53 knockdown prevents the effect of Rho inhibition on reversing the IR-resistant phenotype of IR R-1 cells exposed to different doses of IR. **I** Schematic model of GBM resistance acquisition and reversion by targeting of the Rho and p53 pathways. Illustrations were created with BioRender.com. The immunoblot images are representative of three independent experiments. Immunofluorescence images were acquired with a 63x objective in a high-throughput image acquisition system, and the scale bars represent 10 μM. The graphs show the mean ± SD of at least three independent experiments, with individual replicate dots, as analyzed by two-way ANOVA with Sidak's multiple comparison test.

reversal of acquired radioresistance in GBM tumors with a wild-type p53 genotype.

DATA AVAILABILITY

The databases used in the bioinformatic analyses are available on online platforms, as described in the Materials and Methods section. Uncropped images of the Western blot membranes are available in the Original Data file. All other data are available from the corresponding author.

REFERENCES

1. Bruno F, Pellerino A, Palmiero R, Bertero L, Mantovani C, Garbossa D, et al. Glioblastoma in the elderly: review of Molecular and therapeutic aspects. Biomedicines. 2022;10:644.
2. Olivier C, Oliver L, Lalier L, Vallette FM. Drug resistance in Glioblastoma: the two faces of oxidative stress. Front Mol Biosci. 2021;7:468.
3. Yuan B, Wang G, Tang X, Tong A, Zhou L. Immunotherapy of glioblastoma: recent advances and future prospects. Hum Vaccin Immunother. 2022. https://doi.org/10.1080/21645515.2022.2055417.
4. Bastiancich C, Danhier P, Préat V, Danhier F. Anticancer drug-loaded hydrogels as drug delivery systems for the local treatment of glioblastoma. J Controlled Release. 2016;243:29–42.
5. Osuka S, Zhu D, Zhang Z, Li C, Stackhouse CT, Sampetrean O, et al. N-cadherin upregulation mediates adaptive radioresistance in glioblastoma. J Clin Investig. 2021. https://doi.org/10.1172/JCI136098.
6. Bao S, Wu Q, McLendon RE, Hao Y, Shi Q, Hjelmeland AB, et al. Glioma stem cells promote radioresistance by preferential activation of the DNA damage response. Nature. 2006;444:756–60.
7. Ali MY, Oliva CR, Noman ASM, Allen BG, Goswami PC, Zakharia Y, et al. Radioresistance in glioblastoma and the development of radiosensitizers. Cancers (Basel). 2020;12:2511.
8. Zhang Y, Dube C, Gibert M, Cruickshanks N, Wang B, Coughlan M, et al. The p53 pathway in glioblastoma. Cancers (Basel). 2018. https://doi.org/10.3390/cancers10090297.
9. Goldstein M, Kastan MB. The DNA damage response: Implications for tumor responses to radiation and chemotherapy. Annu Rev Med. 2015;66:129–43.
10. de Gooijer MC, Guillén Navarro M, Bernards R, Wurdinger T, van Tellingen O. An experimenter's guide to glioblastoma invasion pathways. Trends Mol Med. 2018;24:763–80.
11. Magalhaes YT, Farias JO, Silva LE, Forti FL. GTPases, genome, actin: a hidden story in DNA damage response and repair mechanisms. DNA Repair (Amst). 2021;100:103070.
12. Schrank BR, Aparicio T, Li Y, Chang W, Chait BT, Gundersen GG, et al. Nuclear ARP2/3 drives DNA break clustering for homology-directed repair. Nature. 2018;559:61–66.
13. Magalhaes YT, Cardella GD, Forti FL. Exoenzyme C3 transferase lowers actin cytoskeleton dynamics, genomic stability and survival of malignant melanoma cells under UV-light stress. J Photochem Photobiol B. 2020;209:111947.
14. Fritz G, Henninger C. Rho GTPases: novel players in the regulation of the DNA damage response? Biomolecules. 2015;5:2417–34.
15. Magalhaes YT, Silva GET, Osaki JH, Rocha CRR, Forti FL. RHOAming through the nucleotide excision repair pathway as a mechanism of cellular response against the effects of UV radiation. Front Cell Dev Biol. 2020;8:816.
16. Osaki JH, Espinha G, Magalhaes YT, Forti FL. Modulation of RhoA GTPase activity sensitizes human cervix carcinoma cells to γ -radiation by attenuating DNA repair pathways. Oxid Med Cell Longev. 2016;2016:1–11.
17. Espinha G, Osaki JH, Magalhaes YT, Forti FL. Rac1 GTPase-deficient HeLa cells present reduced DNA repair, proliferation, and survival under UV or gamma irradiation. Mol Cell Biochem. 2015;404:281–97.
18. Eduardo da Silva L, Russo LC, Forti FL. Overactivated Cdc42 acts through Cdc42EP3/Borg2 and NCK to trigger DNA damage response signaling and sensitize cells to DNA-damaging agents. Exp Cell Res. 2020. https://doi.org/10.1016/j.yexcr.2020.112206.
19. Dias Gomes M, Letzian S, Saynisch M, Iden S. Polarity signaling ensures epidermal homeostasis by coupling cellular mechanics and genomic integrity. Nat Commun. 2019. https://doi.org/10.1038/s41467-019-11325-3.
20. Arsic N, Ho-Pun-Cheung A, Evelyne C, Assenat E, Jarlier M, Anguille C, et al. The p53 isoform delta133p53β regulates cancer cell apoptosis in a RhoB-dependent manner. PLoS One. 2017. https://doi.org/10.1371/journal.pone.0172125.
21. Yao W, Cai X, Liu C, Qin Y, Cheng H, Ji S, et al. Profilin 1 potentiates apoptosis induced by staurosporine in cancer cells. Curr Mol Med. 2013;13:417–28.
22. Hsu F-F, Lin T-Y, Chen J-Y, Shieh S-Y. p53-Mediated transactivation of LIMK2b links actin dynamics to cell cycle checkpoint control. Oncogene. 2010;29:2864–76.
23. Croft DR, Crighton D, Samuel MS, Lourenco FC, Munro J, Wood J, et al. p53-mediated transcriptional regulation and activation of the actin cytoskeleton regulatory RhoC to LIMK2 signaling pathway promotes cell survival. Cell Res. 2011;21:666–82.
24. Mizuarai S, Yamanaka K, Kotani H. Mutant p53 induces the GEF-H1 oncogene, a guanine nucleotide exchange factor-H1 for RhoA, resulting in accelerated cell proliferation in tumor cells. Cancer Res. 2006;66:6319–26.
25. Krendel M, Zenke FT, Bokoch GM. Nucleotide exchange factor GEF-H1 mediates cross-talk between microtubules and the actin cytoskeleton. Nat Cell Biol. 2002;4:294–301.
26. Gadea G, de Toledo M, Anguille C, Roux P. Loss of p53 promotes RhoA-ROCK-dependent cell migration and invasion in 3D matrices. J Cell Biol. 2007;178:23–30.
27. Xu J, Jiao J, Xu W, Ji L, Jiang D, Xie S, et al. Mutant p53 promotes cell spreading and migration via ARHGAP44. Sci China Life Sci. 2017;60:1019–29.
28. Yu J, Baron V, Mercola D, Mustelin T, Adamson ED. A network of p73, p53 and Egr1 is required for efficient apoptosis in tumor cells. Cell Death Differ. 2007;14:436–46.
29. Magalhaes YT, Farias JO, Monteiro LF, Forti FL. Measuring the contributions of the Rho pathway to the DNA damage response in tumor epithelial cells. Methods Mol Biol. 2018;1821:339–55.
30. Russo LC, Tomasin R, Matos IA, Manucci AC, Sowa ST, Dale K, et al. The SARS-CoV-2 Nsp3 macrodomain reverses PARP9/DTX3L-dependent ADP-ribosylation induced by interferon signaling. J Biol Chem. 2021. https://doi.org/10.1016/j.jbc.2021.101041.
31. Liang X, Guo Y, Figg WD, Fojo AT, Mueller MD, Yu JJ. The role of wild-type p53 in cisplatin-induced Chk2 phosphorylation and the inhibition of platinum resistance with a Chk2 inhibitor. Chemother Res Pract. 2011;2011:1–8.
32. Patyka M, Sharifi Z, Petrecca K, Mansure J, Jean-Claude B, Sabri S. Sensitivity to PRIMA-1MET is associated with decreased MGMT in human glioblastoma cells and glioblastoma stem cells irrespective of p53 status. Oncotarget. 2016;7:60245–69.
33. Wang L, Wang M, Wang S, Qi T, Guo L, Li J, et al. Actin polymerization negatively regulates p53 function by impairing its nuclear import in response to DNA damage. PLoS One. 2013;8:e60179.
34. Qi W, Li J, Pei X, Ke Y, Bu Q, Ni X. β-Actin facilitates etoposide-induced p53 nuclear import. J Biosci. 2020;45:1–8.

35. Saha T, Guha D, Manna A, Panda AK, Bhat J, Chatterjee S, et al. G-actin guides p53 nuclear transport: potential contribution of monomeric actin in altered localization of mutant p53. Sci Rep. 2016;6:32626.
36. Kim JG, Islam R, Cho JY, Jeong H, Cap KC, Park Y, et al. Regulation of RhoA GTPase and various transcription factors in the RhoA pathway. J Cell Physiol. 2018;233:6381–92.
37. Talamillo A, Grande L, Ruiz-Ontanon P, Velasquez C, Mollinedo P, Torices S, et al. ODZ1 allows glioblastoma to sustain invasiveness through a Myc-dependent transcriptional upregulation of RhoA. Oncogene. 2016. https://doi.org/10.1038/onc.2016.341.
38. Kreider-Letterman G, Carr NM, Garcia-Mata R. Fixing the GAP: the role of RhoGAPs in cancer. Eur J Cell Biol. 2022;101:151209.
39. Nai S, Shi Y, Ru H, Ding Y, Geng Q, Li Z, et al. Chk2-dependent phosphorylation of myosin phosphatase targeting subunit 1 (MYPT1) regulates centrosome maturation. Cell Cycle. 2019;18:2651.
40. Zannini L, Delia D, Buscemi G. CHK2 kinase in the DNA damage response and beyond. J Mol Cell Biol. 2014;6:442–57.
41. Blackford AN, Jackson SP. ATM, ATR, and DNA-PK: the trinity at the heart of the DNA damage response. Mol Cell. 2017;66:801–17.
42. Lei T, Du S, Peng Z, Chen L. Multifaceted regulation and functions of 53BP1 in NHEJ-mediated DSB repair (Review). Int J Mol Med. 2022;50:1–19.
43. Lamm N, Rogers S, Cesare AJ. Chromatin mobility and relocation in DNA repair. Trends Cell Biol. 2021;31:843–55.
44. Lamm N, Read MN, Nobis M, van Ly D, Page SG, Masamsetti VP, et al. Nuclear F-actin counteracts nuclear deformation and promotes fork repair during replication stress. Nat Cell Biol. 2020;22:1460–70.
45. ClinicalTrials.gov. A study of APR-246 in oesophageal cancer. 2021 https://www.clinicaltrials.gov/ct2/show/NCT02999893. Accessed 12 Feb 2023.
46. Sallman DA, DeZern AE, Garcia-Manero G, Steensma DP, Roboz GJ, Sekeres MA, et al. Eprenetapopt (APR-246) and azacitidine in TP53-mutant myelodysplastic syndromes. J Clin Oncol. 2021;39:1584–94.
47. Bykov VJN, Eriksson SE, Bianchi J, Wiman KG. Targeting mutant p53 for efficient cancer therapy. Nat Rev Cancer. 2017;18:89–102.
48. ClinicalTrials.gov. Safety study of APR-246 in patients with refractory hematologic cancer or prostate cancer. https://www.clinicaltrials.gov/ct2/show/NCT00900614. Accessed 12 Feb 2023.
49. Wheeler AP, Ridley AJ. Why three Rho proteins? RhoA, RhoB, RhoC, and cell motility. Exp Cell Res. 2004;301:43–49.
50. RhoA RidleyAJ. RhoB and RhoC have different roles in cancer cell migration. J Microsc. 2013;251:242–9.
51. Tseliou M, Al-Qahtani A, Alarifi S, Alkahtani SH, Stournaras C, Sourvinos G. The role of RhoA, RhoB and RhoC GTPases in cell morphology, proliferation and migration in Human Cytomegalovirus (HCMV) infected glioblastoma cells. Cellular Physiol Biochem. 2016;38:94–109.

ACKNOWLEDGEMENTS

The authors thank Prof. Elza T. S. Hojo from the Pharmaceutical Science Faculty of Ribeirão Preto—University of São Paulo, as well as Prof. Carlos F. M. Menck and Dr. Veridiana Munford from the Institute of Biomedical Sciences—University of São Paulo, for the donation and validation of the cell lines and for the support with the cytometer analysis. We thank Prof. Alexandre B. Cardoso and Prof. Nicolas C. Hoch from the Institute of Chemistry—University of São Paulo for the use of Leica DMi8 widefield and Zeiss LSM 780 confocal microscopes, respectively. We also thank Prof. Bianca S. Zingales and the technician Marcelo N. Silva from the Institute of Chemistry—University of São Paulo for equipment usage and reagent exchange.

AUTHOR CONTRIBUTIONS

Conception and design: Y.T.M., F.L.F. Development of methodology: Y.T.M., V.K.B., G.D.C., F.L.F. Acquisition of data: Y.T.M., V.K.B, G.D.C., F.L.F. Analysis and interpretation of data: Y.T.M., V.K.B, G.D.C., F.L.F Writing, review, and/or revision of the manuscript: Y.T.M., V.K.B, F.L.F Administrative, technical, or material support: Y.T.M., F.L.F Study supervision: F.L.F.

FUNDING

This work was supported by grants from the Sao Paulo Foundation—FAPESP (Grant Nos. 2008/58264-5, 2015/03983-0, 2018/01753-6, and 2022/04243-1), Coordenação de Aperfeiçoamento de Pessoal de Nível Superior—CAPES (Grant No. 88887.136364/2017-00) and the National Council for Scientific and Technological Development—CNPq (Grant No. 230420/2016/7) to F.L.F. Y.T.M. is recipient of a FAPESP PhD fellowship (Grant No. 2017/01451-7).

COMPETING INTERESTS

The authors declare no competing interests.

ADDITIONAL INFORMATION

Supplementary information The online version contains supplementary material available at https://doi.org/10.1038/s41419-023-05812-1.

Correspondence and requests for materials should be addressed to Fabio Luis Forti.

Reprints and permission information is available at http://www.nature.com/reprints

Publisher's note Springer Nature remains neutral with regard to jurisdictional claims in published maps and institutional affiliations.